



**HAL**  
open science

## High sensitivity CRDS of the $\alpha 1DgX3Sg$ band of oxygen near $1.27 \mu\text{m}$ : Extended observations, quadrupole transitions, hot bands and minor isotopologues

Olga Leshchishina, Samir Kassi, I. E. Gordon, L. S. Rothman, Wang Le, Alain Campargue

► **To cite this version:**

Olga Leshchishina, Samir Kassi, I. E. Gordon, L. S. Rothman, Wang Le, et al.. High sensitivity CRDS of the  $\alpha 1DgX3Sg$  band of oxygen near  $1.27 \mu\text{m}$ : Extended observations, quadrupole transitions, hot bands and minor isotopologues. *Journal of Quantitative Spectroscopy and Radiative Transfer*, 2010, 111, pp.2236. 10.1016/j.jqsrt.2010.05.014 . hal-00563120

**HAL Id: hal-00563120**

**<https://hal.science/hal-00563120>**

Submitted on 7 Feb 2011

**HAL** is a multi-disciplinary open access archive for the deposit and dissemination of scientific research documents, whether they are published or not. The documents may come from teaching and research institutions in France or abroad, or from public or private research centers.

L'archive ouverte pluridisciplinaire **HAL**, est destinée au dépôt et à la diffusion de documents scientifiques de niveau recherche, publiés ou non, émanant des établissements d'enseignement et de recherche français ou étrangers, des laboratoires publics ou privés.

High sensitivity CRDS of the  $a^1\Delta_g - X^3\Sigma_g^-$  band of oxygen near 1.27  $\mu\text{m}$ :  
extended observations, quadrupole transitions, hot bands and minor isotopologues

Olga Leshchishina<sup>a, c</sup>, Samir Kassi<sup>a</sup>, Iouli E. Gordon<sup>b</sup>, Laurence S. Rothman<sup>b</sup>, Le Wang<sup>a</sup>, Alain  
Campargue<sup>a\*</sup>

<sup>a</sup>*Université Joseph Fourier/CNRS, Laboratoire de Spectrométrie Physique,  
38402 Saint-Martin-d'Hères, FRANCE*

<sup>b</sup>*Harvard-Smithsonian Center for Astrophysics, Atomic and Molecular Physics Division, Cambridge  
MA 02138, USA*

<sup>c</sup>*Laboratory of Theoretical Spectroscopy, Zuev Institute of Atmospheric Optics, 1 Akademicheskii  
av., 634021 Tomsk, RUSSIA*

\*Corresponding author: Tel.: +33 4 76 51 43 19; Fax: +33 4 76 63 54 95.

E-mail address: [Alain.CAMPARGUE@ujf-grenoble.fr](mailto:Alain.CAMPARGUE@ujf-grenoble.fr) (Alain CAMPARGUE).

*Keywords:* Oxygen, O<sub>2</sub>, Electric quadrupole, Singlet delta, Cavity ring down spectroscopy

## Abstract

The CW-Cavity Ring Down Spectroscopy (CW-CRDS) technique has been used to record the high sensitivity absorption spectrum of the  $a^1\Delta_g - X^3\Sigma_g^-$  band of oxygen near 1.27  $\mu\text{m}$ . The spectra were obtained between 7640 and 7917  $\text{cm}^{-1}$  with “natural” oxygen and with a sample highly enriched in  $^{18}\text{O}$ . The absolute intensities of 376 and 649 oxygen transitions were measured in the two spectra, respectively. They include the  $a^1\Delta_g - X^3\Sigma_g^-$  (0-0) bands of  $^{16}\text{O}_2$ ,  $^{16}\text{O}^{18}\text{O}$ ,  $^{16}\text{O}^{17}\text{O}$ ,  $^{17}\text{O}^{18}\text{O}$  and  $^{18}\text{O}_2$ . The (0-0) bands of  $^{16}\text{O}_2$  and  $^{18}\text{O}_2$  show weak quadrupole transitions with line intensities ranging from  $1 \times 10^{-30}$  to  $1.9 \times 10^{-28}$   $\text{cm}/\text{molecule}$ . They are accompanied by the  $a^1\Delta_g - X^3\Sigma_g^-$  (1-1) hot bands which are reported for the first time. The line profiles of the transitions of the  $^{16}\text{O}^{17}\text{O}$  and  $^{17}\text{O}^{18}\text{O}$  isotopologues were observed to be broadened due to an unresolved magnetic hyperfine-structure. Accurate spectroscopic parameters of the different energy levels involved in the observed bands were derived from a global fit of the observed line positions, combined with microwave and Raman measurements available in the literature.

## 1. Introduction

The knowledge of accurate spectroscopic parameters for lines in the  $a^1\Delta_g - X^3\Sigma_g^-$  band of oxygen is very important in the field of remote sensing in relation to high-accuracy measurements of atmospheric greenhouse gases such as  $\text{CO}_2$  and  $\text{CH}_4$ . One reason is that due to the uniform mixing of oxygen, the oxygen lines are often used as a benchmark for intensity calibration of atmospheric spectra taken by satellite instruments. Another reason is that taking the ratio of the column abundance of  $\text{CO}_2$  or  $\text{CH}_4$  to that of  $\text{O}_2$  cancels many common systematic errors, especially the ones that are instrument-related [1].

Due to their importance, magnetic dipole transitions in this band were tabulated in the HITRAN database [2] since its inception [3]. Since then these parameters have been continuously updated as HITRAN was evolving. The intensities of the  $a^1\Delta_g - X^3\Sigma_g^-$  (0-0) band for  $^{16}\text{O}_2$  in HITRAN (which were derived using formalism described in Ref. [4] and modified for HITRAN2000 using experimental parameters from Lafferty et al. [5]), however, were found to be inadequate for atmospheric retrievals such as the ones in Ref. [1]. The new list of  $^{16}\text{O}_2$  intensities recently adopted for HITRAN was derived by Orr-Ewing based on experimental results from Newman et al. [6]. These intensities have proven to be more accurate in application to atmospheric retrievals [1]. In order to further improve the quality of retrievals, Washenfelder et al. [1] applied an empirical scaling to HITRAN2008 intensities of  $^{16}\text{O}^{18}\text{O}$  that originated from Ref. [4]. These intensity improvements have served as a basis for an interim update of the HITRAN oxygen file that was placed on the HITRAN website (<http://www.cfa.harvard.edu/hitrان/updates.html>) in November, 2009. Despite recent updates, there is still significant room for improvement of spectral parameters of the  $a^1\Delta_g - X^3\Sigma_g^-$  band of molecular oxygen. For instance, recently Gordon et al. [7] have shown the necessity of including electric quadrupole lines in this region to the HITRAN line list in order to improve the residuals of the atmospheric solar spectrum. Furthermore, the intensities of  $^{16}\text{O}^{18}\text{O}$  lines in the updated 2009 HITRAN file, while being better than those in the official release of HITRAN2008, are still in need of further improvements.

In the derivation of the current  $a^1\Delta_g - X^3\Sigma_g^-$  line positions of  $^{16}\text{O}_2$  in HITRAN, the  $X^3\Sigma_g^-$  spectroscopic constants from Rouillé et al. [8] and  $a^1\Delta_g$  rotational constants determined from the microwave spectrum by Hillig et al. [9] were used [4]. Ref. [4] states that the term energy of

$a^1\Delta_g$  was taken from Krupenie [10]. However, although none of the subsequent HITRAN papers have elaborated on this, the term values of Krupenie were adjusted in HITRAN to match unpublished FTS spectrum measured by Brault [11]. The effective term values were 7883.75639  $\text{cm}^{-1}$  for  $v=0$  and 9367.20879  $\text{cm}^{-1}$  for  $v=1$ . In HITRAN 2008, the line positions of  $^{16}\text{O}^{18}\text{O}$  were calculated using ground-state constants of Mizushima and Yamomoto [12] and excited-state rotational constants reported by Herzberg and Herzberg [13]. Just like for the principal isotopologue, the term values of Krupenie [10] were adjusted to match unpublished FTS spectrum [11] (the effective value was 7885.06858  $\text{cm}^{-1}$ ).

Although the resulting HITRAN line positions have not received criticism from the users and the quality of the input constants (especially for  $^{16}\text{O}_2$ ) is quite reasonable, it seems that direct measurements of  $a^1\Delta_g - X^3\Sigma_g^-$  band may provide means of obtaining a more consistent set of line positions. Moreover, line positions reported in the most recent measurements by Cheah et al. [14] differ from those in HITRAN by more than 0.01  $\text{cm}^{-1}$ . The authors of Ref. [14] stated that their line positions were superior to the corresponding ones in HITRAN. This disagreement between data also calls for additional experimental studies.

In order to attend the problems listed above and extend the observations, spectra of the  $a^1\Delta_g - X^3\Sigma_g^-$  electronic transitions have been recorded by CW-Cavity Ring Down Spectroscopy (CW-CRDS) in this work. Using two oxygen samples, new spectroscopic information was obtained for five isotopologues, including  $^{16}\text{O}^{17}\text{O}$  for which the  $a^1\Delta_g - X^3\Sigma_g^-$  band is not currently listed in HITRAN, and the  $^{17}\text{O}^{18}\text{O}$  species for which no spectroscopic data in the  $a^1\Delta_g$  state was available previously.

## 2. Experimental details and sample composition

The high-sensitivity CW-CRDS absorption spectra of  $\text{O}_2$  isotopologues were recorded in the 7640-7917  $\text{cm}^{-1}$  region. Two samples were used: the first one contained oxygen with an isotopic composition near natural abundance (hereafter referred to as  $^{16}\text{O}$  sample) and the second one (hereafter referred as  $^{18}\text{O}$  sample) was a sample highly enriched in  $^{18}\text{O}$  (Cambridge Isotope laboratories, >95 % of  $^{18}\text{O}_2$ ). The pressure value of the recordings was fixed to 50.0 Torr. Additional spectra of the  $^{18}\text{O}$  sample were recorded at 5.0 Torr in the 7876-7900  $\text{cm}^{-1}$  region corresponding to the strongest lines, since some of them were saturated at 50.0 Torr.

The fibered distributed feedback (DFB) laser CW-CRDS spectrometer used for these recordings has been described in Refs. [15-17]. Each DFB laser diode has a typical tuning range of about  $40 \text{ cm}^{-1}$  by temperature tuning from  $-5^\circ\text{C}$  to  $60^\circ\text{C}$ . For the present experiment, nine DFB laser diodes were needed to cover the  $7640\text{-}7917 \text{ cm}^{-1}$  region of interest.

The electro-polished stainless steel ringdown cell ( $l = 1.42 \text{ m}$ , inner diameter  $\Phi = 11 \text{ mm}$ ) was fitted by a pair of super-mirrors. The reflectivity of these mirrors (about 99.997 %) corresponds to empty cell ring down times of about  $\tau \sim 200 \text{ }\mu\text{s}$ . About one hundred ringdown events were averaged for each spectral data point; the complete temperature scan of one DFB laser (15000 spectral points) required about 70 minutes. The achieved noise equivalent absorption was about  $\alpha_{min} \sim 4 \times 10^{-11} \text{ cm}^{-1}$  over the whole spectrum. The pressure measured by a capacitance gauge (MKS 100 Torr full range with 0.1% accuracy) and the ringdown cell temperature were monitored during the spectrum recording. **Fig. 1** shows the overview of the two spectra recorded at a pressure of 50.0 Torr and a temperature of 300.2 K. The spectrum does not cover the high energy part of the  $a^1\Delta_g - X^3\Sigma_g^-$  band above  $7917 \text{ cm}^{-1}$  as no fibered DFB laser could be purchased for this spectral region.

Each  $40 \text{ cm}^{-1}$  wide spectrum recorded with one DFB laser was calibrated independently on the basis of the wavelength values provided by a Michelson-type wavemeter (Burleigh WA-1650, 60 MHz resolution and 100 MHz accuracy). The calibration was further refined by stretching the whole spectrum in order to match accurate positions of reference lines (see Ref. [17] for details). The magnetic dipole line positions of the  $a^1\Delta_g - X^3\Sigma_g^-$  band of  $^{16}\text{O}_2$  as provided in the recent HITRAN update [2] were used for calibration. The typical uncertainty in the line positions is estimated to be less than  $1 \times 10^{-3} \text{ cm}^{-1}$ . The spectra of the  $^{18}\text{O}$  sample were calibrated against  $^{16}\text{O}^{18}\text{O}$  lines observed in the spectra of the  $^{16}\text{O}$  sample. In that way the calibration of the two spectra was consistent with the HITRAN line list of  $\text{O}_2$ . The line positions of  $^{16}\text{O}^{18}\text{O}$  from HITRAN were not used for calibration because the quality of the constants used to generate that list were inferior to those used for the principal isotopologue.

The line centers and intensities were determined by using an interactive least squares multi-line fitting program (<http://sourceforge.net/projects/fityk/> version v0.8.6). At 50.0 Torr, the pressure broadening has a significant contribution to the observed line profile and a Voigt function was adopted for the fitting. The DFB linewidth is about one thousandth of the Doppler broadening and thus negligible. The local baseline (assumed to be a linear function of the

wavenumber) and the three parameters of each Voigt profile (line centre, integrated absorbance, HWHM of the Lorentzian component) were fitted. In **Fig. 2**, the spectrum of the  $^{18}\text{O}_2$  Q(19)R(18) magnetic dipole transition at  $7880.215\text{ cm}^{-1}$  is presented with the corresponding residuals. For such well isolated lines, the uncertainty on the retrieved intensity value is estimated to be less than 2%.

Transitions due to the 66, 68 and 67 isotopologues were identified in the  $^{16}\text{O}$  sample, while the 88, 68, 78 and 66 isotopologues were found to contribute to the  $^{18}\text{O}$  spectrum (see Table 1 for the HITRAN shorthand notations of the various isotopologues).

On the basis of the HITRAN intensity values, we checked that the abundance of the  $^{16}\text{O}^{18}\text{O}$  species in the  $^{16}\text{O}$  sample was close to its “natural” value ( $3.77\times 10^{-3}$  against  $3.99\times 10^{-3}$  [2]). The relative abundances of the  $^{16}\text{O}^{18}\text{O}$  and  $^{16}\text{O}_2$  species in the  $^{18}\text{O}$  sample were calculated to be 4.9% and 0.1%, respectively. In order to estimate the relative concentration of the  $^{16}\text{O}^{17}\text{O}$  and  $^{17}\text{O}^{18}\text{O}$  species, we assumed that the band strength was the same as that of the  $^{16}\text{O}^{18}\text{O}$  species. Estimated values of  $7.9\times 10^{-4}$  and 1.1% were obtained for  $^{16}\text{O}^{17}\text{O}$  in the  $^{16}\text{O}$  sample and for  $^{17}\text{O}^{18}\text{O}$  in the  $^{18}\text{O}$  sample, respectively. The relative concentration of  $\text{H}_2\text{O}$  was calculated to be less than  $3\times 10^{-5}$ . **Table 1** summarizes the observations and composition for the two samples and provides the number of lines corresponding to the different bands together with their intensity range.

### 3. Spectrum assignment

#### 3.1. Theoretical Background

In its ground energy state the oxygen molecule has two unpaired electrons with parallel spin leading to a triplet multiplicity (i.e. the total electron spin  $S=1$ ). The two first excited states,  $a^1\Delta_g$  and  $b^1\Sigma_g^+$  arising from the  $\dots(2s\sigma_u)^2(2p\sigma_g)^2(2p\pi_u)^4(2p\pi_g^*)^2$  lowest electron configuration of oxygen are metastable since electric-dipole transitions from the ground state are triply forbidden by spin, orbital angular momentum and parity selection rules. Until recently it was thought that only magnetic dipole transitions in the  $a^1\Delta_g - X^3\Sigma_g^-$  electronic band are experimentally observable, because electric dipole transition between the  $X^3\Sigma_g^-$  and  $a^1\Delta_g$  states are strictly forbidden while electric quadrupole transitions were anticipated to be extremely weak [18]. This perception has changed when we were able to observe electric quadrupole transitions in solar atmospheric spectra and with CRDS [7].

In the frame of Hund's case (b) coupling, each rotational level ( $N$ ) of the  $X^3\Sigma_g^-$  state of molecular oxygen splits into three spin components labeled by  $J$ , with  $\mathbf{J} = \mathbf{N} + \mathbf{S}$ , where  $\mathbf{J}$  is the total angular momentum,  $\mathbf{N}$  is rotational angular momentum and  $\mathbf{S}$  is the total electron spin. Because the total electron spin in the ground state is equal to 1, spin components of each rotational level  $N$  have values of  $J = N - 1$ ,  $J = N$  and  $J = N + 1$ . In the excited electronic state  $a^1\Delta_g$ , the total electron spin is equal to 0, and  $J$  is always equal to  $N$ . Because the projection of orbital angular momentum onto the molecular axis is not zero ( $A=2$ ), each rotational level is split into two, through double orbital degeneracy called  $\Lambda$ -doubling.

For the symmetric species,  $^{16}\text{O}_2$  and  $^{18}\text{O}_2$ , all rotational levels with total parity (-) are absent in both electronic states because the nuclear spin of  $^{16}\text{O}$  and  $^{18}\text{O}$  is equal to zero. This leaves only one  $\Lambda$ -doubling component of each rotational level in the upper state and only odd rotational levels in the ground state. All rotational levels are allowed for the hetero-nuclear isotopologues.

For the isotopologues containing the  $^{17}\text{O}$  atom, such as  $^{16}\text{O}^{17}\text{O}$  and  $^{17}\text{O}^{18}\text{O}$ , the situation becomes more complicated because  $^{17}\text{O}$  has a nuclear spin  $I=5/2$ . Coupling of the nuclear spin to electron spin in the  $X^3\Sigma_g^-$  state [19] and to the electronic angular momentum in the  $a^1\Delta_g$  state gives rise to a magnetic hyperfine structure. Thus each rotational level is split into six components for  $J$  values higher than 2. As a result of the Doppler broadening, the magnetic hyperfine structure cannot be resolved but it clearly shows up as a broadening of the transitions of the  $^{16}\text{O}^{17}\text{O}$  and  $^{17}\text{O}^{18}\text{O}$  species. **Fig. 3** shows an example of the unresolved hyperfine structure of two  $^{17}\text{O}^{18}\text{O}$  transitions which appear significantly broader than the nearby  $^{16}\text{O}^{18}\text{O}$  transitions.

### 3.2. Symmetric isotopologues: $^{16}\text{O}_2$ and $^{18}\text{O}_2$

The assignments of the (0-0) band of  $^{16}\text{O}_2$  were performed by comparison with the assignments provided in the HITRAN database. The maximum deviations between the HITRAN line positions and our observations are on the order of  $3 \times 10^{-3} \text{ cm}^{-1}$  for the highest rotational transitions. The HITRAN intensity cut off was fixed to  $2 \times 10^{-29} \text{ cm/molecule}$ . Five transitions with intensities below this intensity cut off were detected in our spectra.

The first assignments of the (0-0) band of  $^{18}\text{O}_2$  were performed from a rough simulation based on the  $^{16}\text{O}_2$  band with the frequency axis scaled according of the ratio of the  $B$  rotational constants [20]. The assignments were then iteratively extended during the fit of the spectroscopic parameters (see below).

The magnetic dipole transitions of the  $a^1\Delta_g - X^3\Sigma_g^-$  band follow the  $\Delta J = \pm 1, 0$  selection rule leading to the observation of 9 branches represented by the  $\Delta N(N) \Delta J(J)$  notation:  $P(N)Q(J)$ ,  $R(N)Q(J)$ ,  $Q(N)Q(J)$  corresponding to  $\Delta J = 0$  and  $S(N)R(J)$ ,  $P(N)P(J)$ ,  $Q(N)P(J)$ ,  $R(N)R(J)$ ,  $O(N)P(J)$ ,  $Q(N)R(J)$  with  $\Delta J = \pm 1$ . Electric quadrupole transitions follow the  $\Delta J = \pm 2, \pm 1$  and 0 selection rules, which leads to 15 possible branches, but the  $\Delta J = \pm 1$  and 0 transitions, which coincide with much stronger magnetic dipole transitions, are not observable. Therefore only the  $T(N)S(J)$ ,  $S(N)S(J)$ ,  $R(N)S(J)$ ,  $P(N)O(J)$ ,  $O(N)O(J)$ ,  $N(N)O(J)$  branches with  $\Delta J = \pm 2$  are observable. In fact, the  $S(N)S(J)$  and  $O(N)O(J)$  branches were found to be too weak to be detected in the present recordings, leaving only four observed branches for quadrupole transitions.

As the quadrupole transitions reach upper levels which are accessed through magnetic dipole transitions, their positions can be accurately predicted [7]. Overall, 23 and 22 quadrupole transitions were identified for the  $^{16}\text{O}_2$  and  $^{18}\text{O}_2$  species, respectively. Their measured line intensities range between  $1 \times 10^{-30}$  and  $1.8 \times 10^{-28}$  cm/molecule.

The achieved experimental sensitivity allowed for the first detection of the ( $v''=1 \rightarrow v'=1$ ) hot band of  $^{16}\text{O}_2$  and  $^{18}\text{O}_2$  which has a relative intensity of about  $5 \times 10^{-4}$  compared to the (0-0) band. The assignment of the  $^{16}\text{O}_2$  hot band was performed on the basis of predictions obtained using the constants that are used in HITRAN for the  $X^3\Sigma_g^-$  ( $v=1$ ) [8] and  $a^1\Delta_g$  ( $v=1$ ) [11] levels.

The overview of the three bands assigned to the  $^{16}\text{O}_2$  and  $^{18}\text{O}_2$  isotopologues is presented in [Fig. 4](#).

### 3.3. Asymmetric isotopologues: $^{16}\text{O}^{18}\text{O}$ , $^{16}\text{O}^{17}\text{O}$ and $^{17}\text{O}^{18}\text{O}$

The assignments of the  $^{16}\text{O}^{18}\text{O}$  (0-0) band were obtained by comparison with the 2009 update of HITRAN database and then iteratively extended during the fitting of the spectroscopic parameters. The assignments of the corresponding bands of the  $^{16}\text{O}^{17}\text{O}$  and  $^{17}\text{O}^{18}\text{O}$  isotopologues were performed by analogy with the  $^{16}\text{O}^{18}\text{O}$  band, taking into account the change of the rotational constants [20].

[Fig. 5](#) shows a  $10 \text{ cm}^{-1}$  wide section of the  $^{18}\text{O}$ -spectrum where transitions belonging to seven bands were assigned.

As summarized in [Table 1](#), a total of 376 and 649 transitions of the different oxygen isotopologues were measured in the  $^{16}\text{O}$  and  $^{18}\text{O}$  spectra, respectively. Their intensities span

about 5 orders of magnitude between  $1 \times 10^{-30}$  and  $1 \times 10^{-25}$  cm/molecule. In the case of the  $^{18}\text{O}$ -enriched sample, the total number of lines is larger because of the higher concentration of the minor isotopologues, in particular  $^{16}\text{O}^{18}\text{O}$ . Lines due to impurities (mostly  $\text{H}_2\text{O}$  but also  $\text{N}_2\text{O}$  and HF) were identified in both samples. At the final stage of the analysis, only a few tens of impurity lines with maximum intensity values of  $4 \times 10^{-29}$  cm/molecule were left unassigned.

In [Fig. 6](#), the differences of our wavenumber values and HITRAN values are plotted versus the line intensities for  $^{16}\text{O}_2$  and  $^{16}\text{O}^{18}\text{O}$ . Maximum deviations on the order of  $2 \times 10^{-3}$   $\text{cm}^{-1}$  are noted for the weakest  $^{16}\text{O}_2$  lines corresponding to the highest rotational excitation.

It is important to mention that the systematic comparison of about one hundred  $\text{H}_2\text{O}$  line positions measured in our spectra to the values provided in the HITRAN database shows a systematic shift on the order of  $1.1(7) \times 10^{-3}$   $\text{cm}^{-1}$ , our values being smaller than HITRAN values. Recalling that we used HITRAN line positions of the  $^{16}\text{O}_2$  (0-0) band to calibrate our spectra, it indicates that there is an inconsistency on the order of  $1.1 \times 10^{-3}$   $\text{cm}^{-1}$  between the HITRAN line positions of  $\text{H}_2\text{O}$  and  $\text{O}_2$  in the considered spectral region.

We provide as Supplementary Material the two global line lists including the experimental values of the intensities corresponding to the relative abundance listed in [Table 1](#).

#### 4. Band-by-band fit

The SPFIT software [21] was used to fit all the measured transitions. The ground  $X^3\Sigma_g^-$  electronic state is represented by the following effective Hamiltonian:

$$H_{\text{eff}} = BN^2 - DN^4 + HN^6 + [\lambda + \lambda_D N^2 + \lambda_H N^4] \frac{2}{3} (3S_z^2 - S^2) + [\gamma + \gamma_D N^2 + \gamma_H N^4] \mathbf{N} \cdot \mathbf{S}, \quad (1)$$

where  $B$ ,  $\lambda$  and  $\gamma$  are rotational, spin-spin and spin-rotation interaction constants, respectively, while the other constants are their first and second order centrifugal distortion terms. The rotational energies in the  $a^1\Delta_g$  state were fit to a simple expression:

$$F_v(J) = T_v + B_v J(J+1) - D_v [J(J+1)]^2 + H_v [J(J+1)]^3. \quad (2)$$

One should note that theoretically the second order  $\Lambda$ -doubling term should be added to this equation (see for instance Eq. (2) from the work of Drouin et al. [20]). Nevertheless, although the  $\Lambda$ -doubling splitting of the rotational levels increases as  $\sim J^{2\Omega}$  and for some of the isotopologues the lines with  $J' \leq 43$  were observed, that splitting could not be resolved in our experiments. This is in accord with the findings of Drouin et al. [20] where the microwave (MW)

transitions within the  $a^1\Delta_g$  state involving  $J \leq 23$  were measured. Although Drouin et al. did use the second order  $\Lambda$ -doubling constant in the fit, they found it to be largely undetermined, which (taking into account that these MW measurements are very precise) leads to the conclusion that this constant is negligible. Another difference between Eq. (2) in this paper and Eq. (2) from Ref. [20] is that the powers of  $[J(J+1)]$  are used here instead of  $[J(J+1) - \Omega^2]$ . This, of course, does not affect the quality of the fit and is really a matter of preference. However, this does affect the magnitudes of the fitted constants, especially the term energy  $T_v$ , which will differ by approximately  $B\Omega^2$ , depending on the Hamiltonian used.

#### 4.1. $^{16}\text{O}_2$

The lines of the  $a^1\Delta_g - X^3\Sigma_g^-$  (0-0) and (1-1) bands measured in this work were fitted together with lines from supplementary material of work devoted to THz measurements by Drouin et al. [20]. In addition to transitions within the  $v = 0$  states of ground and  $a^1\Delta_g$  electronic states measured by Drouin et al, their supplementary file includes microwave measurements in the  $X^3\Sigma_g^-$  state by Tretyakov et al. [22], Endo and Mizushima [23], Golubiatnikov and Krupnov [24], Zink and Mizushima [25] and Park et al. [26] as well as MW measurements in the  $a^1\Delta_g$  state by Hillig et al. [9]. We have also included MW measurements in the  $X^3\Sigma_g^-$  ( $v = 1$ ) [23] and  $a^1\Delta_g$  ( $v = 1$ ) [27] states. In order to connect all four vibrational states ( $X^3\Sigma_g^-$   $v = 0, 1$  and  $a^1\Delta_g$   $v = 0, 1$ ) observed in our work, stimulated Raman measurements of the fundamental band in the  $X^3\Sigma_g^-$  state by Rouillé et al. [8] and Millot et al. [28] were also included. Note that there are also incoherent Raman measurements [29] available in the literature. However, the data available in Ref. [29] does not exceed the one from Rouillé et al. [8], while the experimental uncertainty in Ref. [29] is larger. The reported experimental uncertainty was used for OO and SS branches from Ref. [8]. However, the  $0.001 \text{ cm}^{-1}$  uncertainty reported there for the QQ branch lines seems to be underestimated. The reason is that in the QQ branch of the stimulated Raman spectra the fine structure of the rotational levels is not resolved unlike the OO and SS branches. We therefore assigned line centers reported for QQ branches to all three components of the transition using the option of SPFIT to include blended lines and weight them with calculated relative intensities. The results of the fit are given in Table 2. In Table 3, the  $a^1\Delta_g$  state constants are compared with those from Amiot and Vergès [30], Rothman [31], Cheah et al. [14], Drouin et al. [20] and with the constants used to generate the most recent HITRAN line list. It is worth

noting that in Ref. [31] experimental values from Amiot and Vergès [30] were fit together with (0-0) band higher rotational levels observed in the Venus spectra of Ref. [32] and (1-0) transitions from the Liège Atlas data [33]. Significant differences can be immediately noted in term energies ( $T$ ) of  $a^1\Delta_g$  determined in Refs. [14] and [31] and the ones determined in Ref. [30]. The values from Ref. [14] were derived using a different Hamiltonian than Eq. (2) of this paper. Cheah et al. [14] used  $[J(J+1) - \Omega^2]$  whereas we used just  $J(J+1)$ . Also, Cheah et al. [14] and Rothman [31] have taken the zero point energy for the first existing energy level in the symmetric species of oxygen of the ground state ( $N = 1, J = 0$ ), whereas in this work and the work of Amiot and Vergès [30], the hypothetical  $N = 0, J = 1$  level for these species was taken as zero. Another interesting observation is that the rotational constants  $H$  in this work and Ref. [30] are not only significantly different in magnitude but also in sign. Finally, one can note that the line positions from Ref. [14] are systematically larger than ours by  $\sim 0.02 \text{ cm}^{-1}$  with a maximum deviation of  $0.050 \text{ cm}^{-1}$  for one line of the QQ branch. It is hard to explain this discrepancy but the line positions measured here agree well if calibrated using HITRAN water or HITRAN oxygen lines, which provides confidence in our measurements.

Table 2 includes the *rms* values of the fit corresponding to the different experimental

sources (MW, Raman and this work) :  $rms = \sqrt{\frac{\sum_i (\sigma_{obs} - \sigma_{calc})_i^2}{N - p}}$ , where the summation applies

to the  $N$  experimental data of a given source and  $p$  is the number of fitted parameters. The *rms* value corresponding to our data is  $1.13 \times 10^{-3} \text{ cm}^{-1}$  in agreement with our experimental uncertainty.

#### 4.2. $^{18}\text{O}_2$

In the same manner as the principal isotopologue,  $^{18}\text{O}_2$  lines of the  $a^1\Delta_g - X^3\Sigma_g^-$  (0-0) and (1-1) bands observed in this work were fitted together with lines from supplementary material of work by Drouin et al. [20], which also contains measurements within the  $\nu = 0$  state of  $X^3\Sigma_g^-$  by Endo and Mizushima [34] and Steinbach and Gordy [35]. In addition we have included the measurements within the  $X^3\Sigma_g^-$  ( $\nu = 1$ ) state [34] and within the  $a^1\Delta_g$  ( $\nu = 0$ ) state [27]. Raman measurements of the fundamental band in the  $X^3\Sigma_g^-$  state by Edwards et al. [36] were also included to connect vibrational levels in both electronic states. Unlike the Raman measurements of  $^{16}\text{O}_2$  by Rouillé et al. [8], the fine structure was not resolved by Edwards et al. not only for the

QQ branch but also for the OO and SS branches. We therefore assigned large uncertainties (up to  $0.05 \text{ cm}^{-1}$ ) to the Raman line centers. This resulted in a less accurate determination of the absolute energy term values of  $X^3\Sigma_g^- (v=1)$  and  $a^1\Delta_g (v=1)$  states than for  $^{16}\text{O}_2$ . The results of the fit are summarized in [Table 4](#). The *rms* values of the Raman data and our near infrared data ( $6.8 \times 10^{-2}$  and  $7.7 \times 10^{-4} \text{ cm}^{-1}$ , respectively) reflect the accuracy of the two experimental sources.

#### 4.3. $^{16}\text{O}^{18}\text{O}$

$^{16}\text{O}^{18}\text{O}$  transitions were observed in both experiments ( $^{16}\text{O}$  and  $^{18}\text{O}$  samples). As mentioned above, the spectrum of the  $^{18}\text{O}$  sample had more  $^{16}\text{O}^{18}\text{O}$  lines as a result of a higher relative concentration. These were used as a primary source of the measured data. We did however add a few  $^{16}\text{O}^{18}\text{O}$  lines from the  $^{16}\text{O}_2$  spectra when the corresponding transitions were blended in the  $^{18}\text{O}_2$  spectra. Once again the supplementary material of work by Drouin et al. [20] was employed in the fit together with our measurements. For  $^{16}\text{O}^{18}\text{O}$ , that file also contains measurements within the  $X^3\Sigma_g^- (v=0)$  state by Amano and Hirota [37], Mizushima and Yamamoto [12], Steinbach and Gordy [38] and Crownover et al. [39]. We have also added the MW measurements within  $a^1\Delta_g (v=0)$  state by Cohen et al. [27]. The results of the fit are summarized in [Table 4](#).

#### 4.4. $^{16}\text{O}^{17}\text{O}$ and $^{17}\text{O}^{18}\text{O}$

Transitions of the  $^{16}\text{O}^{17}\text{O}$  isotopologue were identified in the spectrum of the  $^{16}\text{O}$  sample while transitions of  $^{17}\text{O}^{18}\text{O}$  were observed in the  $^{18}\text{O}$  spectrum. These transitions are very weak, which increases the experimental uncertainty in determination of line centers. Furthermore, these lines were often wider than the lines from other isotopologues (see [Fig. 3](#)) and sometimes appear asymmetric. As mentioned above, this is due to the unresolved hyperfine structure. Indeed, the nuclear spin of  $^{17}\text{O}$  is  $5/2$  which results in the splitting of each fine structure component into six hyperfine sublevels. The hyperfine splitting in the ground  $X^3\Sigma_g^-$  state of  $^{16}\text{O}^{17}\text{O}$  and  $^{17}\text{O}^{18}\text{O}$  is significant as determined by Cazzoli et al. [19], and is expected to be even larger in the excited state through coupling of electronic angular momentum and nuclear spin [40]. Therefore the hyperfine splitting of the energy levels is sufficient to make the lines in the electronic spectrum wider, but insufficient to be completely resolved under our experimental conditions. Line broadening due to unresolved hyperfine structure in infrared and electronic spectra is fairly common and was observed in the low-rotational lines of the infrared spectrum of MnH, for

example [41]. To minimize the negative effect of unresolved hyperfine structure, the line positions were taken as the average value over the line profile of the wavenumbers weighted by the corresponding absorption coefficient. As a consequence, the uncertainties assigned to the  $^{16}\text{O}^{17}\text{O}$  and  $^{17}\text{O}^{18}\text{O}$  transitions were increased up to  $3 \times 10^{-3} \text{ cm}^{-1}$ .

When performing similar analyses of the A-band lines of  $^{16}\text{O}^{17}\text{O}$  and  $^{17}\text{O}^{18}\text{O}$ , Robichaud et al. [42] fixed the ground state constants to the ones determined by Cazzoli et al. [19]. This procedure is fairly common and is based on the fact that microwave measurements are usually more accurate. There are, however, obstacles in this particular case. First, the MW data of Cazzoli et al. do not go beyond  $N = 12$ , while the data recorded in this work exceeds  $N = 20$ . Second, the centrifugal distortion constant  $D$  could not have been well determined from the fit, since the measurements were performed only between fine structure components of the same rotational levels [19]. The value of  $D$  reported by Cazzoli et al. is an estimate based on isotopic scaling of the well known value for  $^{16}\text{O}_2$ . The measurement in the A-band [41] could not help determining the  $D$  value in the ground state either because only P-lines were measured in that work.

In this work the MW lines from Cazzoli et al [19] were fit together with electronic transitions. The hyperfine structure resolved in the ground state was fit to

$$H_{hfs} = b_F \mathbf{I} \cdot \mathbf{S} + c(\mathbf{I}_z \mathbf{S}_z - \frac{1}{3} \mathbf{I} \cdot \mathbf{S}) + \frac{e^2 Qq(3I_z^2 - I(I+1))}{4I(2I-1)}, \quad (3)$$

where  $b_F$  is a Fermi contact parameter,  $c$  is a dipolar parameter, and  $eQq$  is electric quadrupole interaction parameter.

In the first iteration of the combined fit, we determined the centrifugal distortion constant  $D$  in the ground state. We then fixed that constant to its fitted value and fit only the data from Ref. [19] with the same amount of constants as in that work. The results of the fit are given in **Table 5**. Surprisingly, the fit have yielded much better determined rotational and hyperfine constants than in the original paper. We then fixed the new ground state constants and performed the fit of only electronic transitions measured in this work. In such a way we determined previously unavailable constants for the  $a^1\Delta_g$  state of  $^{16}\text{O}^{17}\text{O}$  and  $^{17}\text{O}^{18}\text{O}$  (see Table 4). The corresponding *rms* values relative to our data ( $2.35 \times 10^{-3} \text{ cm}^{-1}$  and  $2.57 \times 10^{-3} \text{ cm}^{-1}$  for  $^{16}\text{O}^{17}\text{O}$  and  $^{17}\text{O}^{18}\text{O}$ , respectively) are satisfactory considering the larger uncertainty on the line centers.

The results of the fit of the spectroscopic parameters of each of the five isotopologues under consideration are provided as Supplementary Material. The supplementary files include the complete set of wavenumber values used to refine the parameters together with the corresponding fitted values and reference. The files relative to the  $^{16}\text{O}^{17}\text{O}$  and  $^{17}\text{O}^{18}\text{O}$  species include the results of the new fit of Cazzoli et al. microwave measurements.

## 5. Conclusion

This work was mainly inspired by the deficiencies in the existing reference spectroscopic data for the  $a^1\Delta_g - X^3\Sigma_g^-$  band of molecular oxygen which is very important in atmospheric studies. The obtained results presented here provide information for improving the HITRAN line list both in terms of accuracy and completeness. In Ref. [7], it was shown that it is important to include  $a^1\Delta_g - X^3\Sigma_g^-$  electric quadrupole transitions of  $^{16}\text{O}_2$  into HITRAN in order to improve atmospheric retrievals. The intensities of many of these transitions are actually above the HITRAN intensity cutoff ( $2 \times 10^{-29}$  cm/molecule). The intensities of the (1-1) band of  $^{16}\text{O}_2$  and of the (0-0) band of  $^{16}\text{O}^{17}\text{O}$  measured in this work are comparable with those of the  $^{16}\text{O}_2$  electric quadrupole transitions and also need to be accounted for. Therefore parameters measured here will be used to generate line lists and complete the present HITRAN line list by including bands discussed above and lowering the intensity cut off. The line intensities for  $^{16}\text{O}^{18}\text{O}$  measured here, are of particular importance. The lack of proper experimental input parameters for  $^{16}\text{O}^{18}\text{O}$  was a main reason for limited quality of line intensities in the  $a^1\Delta_g - X^3\Sigma_g^-$  band for these species in HITRAN

Overall, the spectroscopic fit of different  $a^1\Delta_g - X^3\Sigma_g^-$  transitions measured in this work and available microwave and Raman data provides the best set of spectroscopic constants for the  $a^1\Delta_g$  state to date. For the  $^{17}\text{O}^{18}\text{O}$  species, these  $a^1\Delta_g$  parameters were determined for the first time. Also, improved ground state constants (in particular centrifugal distortion) were obtained for the  $^{16}\text{O}^{17}\text{O}$  and  $^{17}\text{O}^{18}\text{O}$  isotopologues.

## Acknowledgments

We are very thankful to Shanshan Yu for her help in using the SPFIT program. Part of this work was performed at Grenoble University under the ANR project “IDEO”

(NT09\_436466). The HITRAN database is supported by NASA through the Earth Observing System (*EOS*) program under the grant NAG5-13534.

## References

- [1] Washenfelder RA, Toon GC, Blavier J-F, Yang Z, Allen NT, Wennberg PO, et al. Carbon dioxide column abundances at the Wisconsin Tall Tower site. *Journal of Geophysical Research (Atmospheres)* 2006;111:22305.
- [2] Rothman LS, Gordon IE, Barbe A, Benner DC, Bernath PF, Birk M, et al. The HITRAN 2008 molecular spectroscopic database. *J Quant Spectrosc Radiat Transfer* 2009;110:533-72.
- [3] McClatchey RA, Benedict WS, Clough SA, Burch DE, Calfee RF, Fox K, et al *AFCRL Atmospheric Absorption Line Parameters Compilation*; 1973.
- [4] Gamache RR, Goldman A, Rothman LS. Improved spectral parameters for the three most abundant isotopomers of the oxygen molecule. *J Quant Spectrosc Radiat Transfer* 1998;59:495-509.
- [5] Lafferty WJ, Solodov AM, Lugez CL, Fraser GT. Rotational Line Strengths and Self-Pressure-Broadening Coefficients for the 1.27  $\mu\text{m}$ ,  $a^1\Delta_g - X^3\Sigma_g^-$  (0,0) Band of  $\text{O}_2$ . *Appl Opt* 1998;37:2264-70.
- [6] Newman SM, Lane IC, Orr-Ewing AJ, Newnham DA, Ballard J. Integrated absorption intensity and Einstein coefficients for the  $\text{O}_2$   $a^1\Delta_g - X^3\Sigma_g^-$  (0,0) transition: A comparison of cavity ringdown and high resolution Fourier transform spectroscopy with a long-path absorption cell. *J Chem Phys* 1999;110:10749-57.
- [7] Gordon IE, Kassi S, Campargue A, Toon GC. First identification of the  $a^1\Delta_g - X^3\Sigma_g^-$  electric quadrupole transitions of oxygen in the solar and laboratory spectra. *J Quant Spectrosc Radiat Transfer* 2010;In Press.
- [8] Rouillé G, Millot G, Saint-Loup R, Berger H. High-resolution stimulated Raman spectroscopy of  $\text{O}_2$ . *J Mol Spectrosc* 1992;154:372-82.
- [9] Hillig KW, Chiu CCW, Read WG, Cohen EA. The pure rotation spectrum of  $a^1\Delta_g$   $\text{O}_2$ . *J Mol Spectrosc* 1985;109:205-6.
- [10] Krupenie PH. The Spectrum of Molecular Oxygen *J Phys Chem Ref Dat* 1972;1:423-534.
- [11] Brault J, private communication, 1982.
- [12] Mizushima M, Yamamoto S. Microwave absorption lines of  $^{16}\text{O}^{18}\text{O}$  in its ( $X^3\Sigma_g^-, v = 0$ ) state. *J Mol Spectrosc* 1991;148:447-52.
- [13] Herzberg L, Herzberg G. Fine Structure of the Infrared Atmospheric Oxygen Bands. *Astrophys J* 1947;105:353.
- [14] Cheah S-L, Lee Y-P, Ogilvie JF. Wavenumbers, strengths, widths and shifts with pressure of lines in four bands of gaseous  $^{16}\text{O}_2$  in the systems  $a^1\Delta_g - X^3\Sigma_g^-$  and  $b^1\Sigma_g^+ - X^3\Sigma_g^-$ . *J Quant Spectrosc Radiat Transfer* 2000;64:467-82.
- [15] Macko P, Romanini D, Mikhailenko SN, Naumenko OV, Kassi S, Jenouvrier A, et al. High sensitivity CW-cavity ring down spectroscopy of water in the region of the 1.5 $\mu\text{m}$  atmospheric window. *Journal of Molecular Spectroscopy* 2004;227:90-108.
- [16] Morville J, Romanini D, Kachanov AA, Chenevier M. Two schemes for trace detection using cavity ringdown spectroscopy. *Appl Phys* 2004;D78:465-76.
- [17] Perevalov BV, Kassi S, Romanini D, Perevalov VI, Tashkun SA, Campargue A. CW-cavity ringdown spectroscopy of carbon dioxide isotopologues near 1.5  $\mu\text{m}$ . *J Mol Spectrosc* 2006;238:241-55.
- [18] Minaev BE, Minaeva VA, Evtuhov YV. Quantum-Chemical Study of the Singlet Oxygen Emission. *Int J Quantum Chem* 2009;109:500-15.

- [19] Cazzoli G, Degli Esposti C, Favero PG, Severi G. Microwave spectra of  $^{16}\text{O}^{17}\text{O}$  and  $^{18}\text{O}^{17}\text{O}$ . *Nuovo Cimento B Serie* 1981;62:243-54.
- [20] Drouin BJ, Yu S, Miller CE, Müller HSP, Lewen F, Brünken S, et al. Terahertz spectroscopy of oxygen,  $\text{O}_2$ , in its  $^3\Sigma$  and  $^1\Delta$  electronic states: THz Spectroscopy of  $\text{O}_2$ . *J Quant Spectrosc Radiat Transfer* 2010;In Press.
- [21] Pickett HM. The fitting and prediction of vibration-rotation spectra with spin interactions. *J Mol Spectrosc* 1991;148:371-7.
- [22] Tretyakov MY, Koshelev MA, Dorovskikh VV, Makarov DS, Rosenkranz PW. 60-GHz oxygen band: precise broadening and central frequencies of fine-structure lines, absolute absorption profile at atmospheric pressure, and revision of mixing coefficients. *J Mol Spectrosc* 2005;231:1-14.
- [23] Endo Y, Mizushima M. Microwave Resonance Lines of  $^{16}\text{O}_2$  in Its Electronic Ground State ( $X^3\Sigma_g^-$ ). *Jpn J Appl Phys* 1982;21:L379-L80.
- [24] Golubiatnikov GY, Krupnov AF. Microwave study of the rotational spectrum of oxygen molecule in the range up to 1.12 THz. *J Mol Spectrosc* 2003;217:282-7.
- [25] Zink LR, Mizushima M. Pure rotational far-infrared transitions of  $^{16}\text{O}_2$  in its electronic and vibrational ground state. *J Mol Spectrosc* 1987;125:154-8.
- [26] Park K, Nolt IG, Steele TC, Zink LR, Evenson KM, Chance KV, et al. Pressure broadening of the 50.873 and 83.469  $\text{cm}^{-1}$  molecular oxygen lines. *J Quant Spectrosc Radiat Transfer* 1996;56:315-6.
- [27] Cohen EA, Okunishi M, Oh JJ. The isotope effect of the  $\text{O}_2$   $a^1\Delta_g$  rotational constant. *J Mol Struct* 1995;352-353:283-7.
- [28] Millot G, Lavorel B, Fanjoux G. Pressure Broadening, Shift, and Interference Effect for a Multiplet Line in the Rovibrational Anisotropic Stimulated Raman Spectrum of Molecular Oxygen. *J Mol Spectrosc* 1996;176:211-8.
- [29] Brodersen S, Bendtsen J. The incoherent Raman spectrum of  $^{16}\text{O}_2$  molecular constants from all experimental data. *J Mol Spectrosc* 2003;219:248-57.
- [30] Amiot C, Vergès J. The magnetic dipole  $a^1\Delta_g - X^3\Sigma_g^-$  transition in the oxygen afterglow. *Can J Phys* 1981;59:1391.
- [31] Rothman LS. Magnetic dipole infrared atmospheric oxygen bands. *Appl Opt* 1982;21:2428-31.
- [32] Connes P, Michel G. High-Resolution Fourier Spectra of Stars and Planets. *Astrophys J* 1974;190:L29.
- [33] Swensson JW, Benedict WS, Delbouille L, Roland G, in: *Mem Soc R Sci Liege Collect Special*, 1970; Vol. 5.
- [34] Endo Y, Mizushima M. Microwave Absorption Lines of  $^{18}\text{O}_2$  in Its Electronic Ground State ( $X^3\Sigma_g^-$ ). *Jpn J Appl Phys* 1983;22:L534-L6.
- [35] Steinbach W, Gordy W. Millimeter and Submillimeter Wave Spectrum of  $^{18}\text{O}_2$  *Phys Rev A* 1973;8:1753-8.
- [36] Edwards HGM, Long DA, Najm KAB, Thomsen M. The vibration-rotation Raman spectra of  $^{18}\text{O}_2$ ,  $^{17}\text{O}^{18}\text{O}$ ,  $^{17}\text{O}_2$  and  $^{16}\text{O}_2$ . *J Raman Spectrosc* 1981;10:60-3.
- [37] Amano T, Hirota E. Microwave spectrum of the molecular oxygen in the excited vibrational state. *J Mol Spectrosc* 1974;53:346-63.
- [38] Steinbach W, Gordy W. Microwave spectrum and molecular constants of  $^{16}\text{O}^{18}\text{O}$  *Phys Rev A* 1975;11:729-31.

- [39] Crownover RL, De Lucia FC, Herbst E. The submillimeter-wave spectrum of  $^{16}\text{O}^{18}\text{O}$ . *Astrophys J* 1990;349:L29-L31.
- [40] Arrington CA, Jr., Falick AM, Myers RJ. Electron Paramagnetic Resonance Spectrum of  $\text{O}_2$  ( $a^1\Delta_g$ )-Its  $^{17}\text{O}$  Hyperfine Coupling and Electronic and Rotational g Values. *J Chem Phys* 1971;55:909-14.
- [41] Gordon IE, Appadoo DRT, Shayesteh A, Walker KA, Bernath PF. Fourier transform infrared emission spectra of MnH and MnD. *Journal of Molecular Spectroscopy* 2005;229:145-9.
- [42] Robichaud DJ, Yeung LY, Long DA, Okumura M, Havey DK, Hodges JT, et al. Experimental Line Parameters of the  $b^1\Sigma_g^+ - X^3\Sigma_g^-$  Band of Oxygen Isotopologues at 760 nm Using Frequency-Stabilized Cavity Ring-Down Spectroscopy. *J Phys Chem A* 2009;113:13089-99.

## Figure captions.

**Figure 1.** Overview of the  $a^1\Delta_g - X^3\Sigma_g^-$  band of oxygen recorded by CW-CRDS ( $P= 50.0$  Torr,  $T= 300.2$  K). The upper and lower panels correspond to  $O_2$  with an isotopic composition near natural abundance sample and a highly  $^{18}O$ -enriched sample, respectively.

**Figure 2.** Spectrum of the  $^{18}O_2$  Q(19)R(18) magnetic dipole transition at  $7880.215\text{ cm}^{-1}$  ( $P= 5.0$  Torr,  $T= 298\text{K}$ ). The upper panel shows the measured (x) and fitted (solid) line profiles; the lower panel shows the residuals of the fit.

**Figure 3.** Apparent line broadening due to the unresolved hyperfine structure of two  $^{17}O^{18}O$  transitions. The  $^{17}O^{18}O$  lines are significantly broader than the nearby  $^{16}O^{18}O$  line.

**Figure 4.** Overview of the absorption spectrum of  $^{16}O_2$  (lower panel) and  $^{18}O_2$  (upper panel) ( $P= 50.0$  Torr). Full circles, open stars and full stars correspond to the  $a^1\Delta_g - X^3\Sigma_g^-$  (0-0) band, the (1-1) hot band and quadrupole transitions, respectively. For completeness, a few lines of  $^{16}O_2$  (0-0) band (light full circles), which were saturated in the CRDS spectrum, have been replaced by the corresponding HITRAN values.

**Figure 5.** A section of the spectrum of the  $^{18}O$ -enriched sample ( $P= 50.0$  Torr,  $T= 300.2$  K) near  $7747\text{ cm}^{-1}$ . Transitions belonging to seven bands of four isotopologues are assigned in the displayed spectral region.

**Figure 6.** Differences between the wavenumbers values measured in this work and those provided in the HITRAN database for  $^{16}O_2$  (upper panel) and  $^{16}O^{18}O$  (lower panel) versus the line intensity. The  $^{16}O^{18}O$  wavenumber values were measured in the spectrum of the  $^{18}O$  enriched sample and the line intensities correspond to the 4.9 % relative abundance of  $^{16}O^{18}O$  in this sample.

**Table 1.**

Summary of the CW-CRDS observations of the  $a^1\Delta_g - X^3\Sigma_g^-$  band of O<sub>2</sub> near 1.27  $\mu\text{m}$ .

Isotopologue	HITRAN notation	Abundance	Band	Number of lines	Intensity range <sup>a</sup> ( $\times 10^{-26}$ cm/molecule)
<sup>16</sup> O sample					
<sup>16</sup> O <sub>2</sub>	66	0.995	(0-0)	97	$3.9 \times 10^{-4} - 11.0$
			(0-0) elec. quad.	23	$1.0 \times 10^{-4} - 1.9 \times 10^{-2}$
			(1-1)	79	$1.1 \times 10^{-4} - 6.4 \times 10^{-3}$
<sup>16</sup> O <sup>18</sup> O	68	$3.8 \times 10^{-3}$	(0-0)	127	$4.3 \times 10^{-4} - 1.9 \times 10^{-2}$
<sup>16</sup> O <sup>17</sup> O	67	$7.9 \times 10^{-4}$	(0-0)	50	$3.1 \times 10^{-4} - 5.8 \times 10^{-3}$
<sup>18</sup> O sample					
<sup>18</sup> O <sub>2</sub>	88	0.94	(0-0)	138	$2.0 \times 10^{-4} - 10.1$
			(0-0) elec. quad.	22	$1.1 \times 10^{-4} - 6.0 \times 10^{-3}$
			(1-1)	95	$1.1 \times 10^{-4} - 8.1 \times 10^{-3}$
<sup>16</sup> O <sup>18</sup> O	68	$4.9 \times 10^{-2}$	(0-0)	202	$1.6 \times 10^{-4} - 3.4 \times 10^{-1}$
<sup>17</sup> O <sup>18</sup> O	78	$\sim 1 \times 10^{-2}$	(0-0)	139	$3.3 \times 10^{-4} - 6.4 \times 10^{-2}$
<sup>16</sup> O <sub>2</sub>	66	$\sim 1 \times 10^{-3}$	(0-0)	53	$1.1 \times 10^{-4} - 1.3 \times 10^{-2}$

<sup>a</sup> The given intensity values include the relative abundance in the considered sample.

**Table 2**Spectroscopic parameters of the  $\nu=0$  and 1 levels of the  $X^3\Sigma_g^-$  and  $a^1\Delta_g$  states of  $^{16}\text{O}_2$  and  $^{18}\text{O}_2$ 

Parameters	$^{16}\text{O}_2$			$^{18}\text{O}_2$		
	$X^3\Sigma_g^-$					
	$\nu=0$		$\nu=1$	$\nu=0$		$\nu=1$
$E^a$	-		1556.389914(147)			1468.4442(33)
$B$	1.437675974(19)		1.42186406(64)	1.278008448(57)		1.2647600(12)
$D$	$4.840356(76)\times 10^{-6}$		$4.83954(42)\times 10^{-6}$	$3.82252(39)\times 10^{-6}$		$3.82558(727)\times 10^{-6}$
$H$				$-5.20(494)\times 10^{-13}$		
$\lambda$	1.984751193(50)		1.98957881(13)	1.9845955423(417)		1.989117019(166)
$\lambda_D$	$1.946930(325)\times 10^{-6}$		$2.11277(98)\times 10^{-6}$	$1.721382(233)\times 10^{-6}$		$1.85292(127)\times 10^{-6}$
$\lambda_H$	$9.71(30)\times 10^{-12}$			$7.719(242)\times 10^{-12}$		$1.614(213)\times 10^{-11}$
$\gamma$	$-8.42537356(584)\times 10^{-3}$		$-8.445758(19)\times 10^{-3}$	$-7.48670002(457)\times 10^{-3}$		$-7.5038322(130)\times 10^{-3}$
$\gamma_D$	$-8.1183(223)\times 10^{-9}$		$-8.349(79)\times 10^{-9}$	$-6.4111(160)\times 10^{-9}$		$-6.4108(267)\times 10^{-9}$
$\gamma_H$	$4.84(153)\times 10^{-14}$			$-3.80(113)\times 10^{-14}$		
	$a^1\Delta_g$					
	$\nu=0$		$\nu=1$	$\nu=0$		$\nu=1$
$T$	7883.756645(113)		9367.208821(267)	7886.409277(117)		9286.2239(33)
$B$	1.417839039(38)		1.40072433(17)	1.260409499(56)		1.2460722(28)
$D$	$5.102256(243)\times 10^{-6}$		$5.1211(41)\times 10^{-6}$	$4.029678(664)\times 10^{-6}$		$4.04700(827)\times 10^{-6}$
$H$	$-2.395(283)\times 10^{-12}$		$-4.97(313)\times 10^{-12}$	$-1.855(617)\times 10^{-12}$		
<b>Number of lines</b>	MW: 85	Raman: 94	This work: 199	MW: 78	Raman: 26	This work: 255
	Total: 378			Total: 359		
<b>rms</b>	$3.48\times 10^{-2}$ MHz	$2.48\times 10^{-3}$ cm $^{-1}$	$1.13\times 10^{-3}$ cm $^{-1}$	$2.48\times 10^{-2}$ MHz	$68.1\times 10^{-3}$ cm $^{-1}$	$0.77\times 10^{-3}$ cm $^{-1}$

**Note**

<sup>a)</sup> The energy origin is taken for the hypothetical  $N=0$   $J=1$  level of the symmetric species of the ground  $X^3\Sigma_g^-$  state (see text for details). The lowest energy level of  $^{16}\text{O}_2$  will be  $0.24584\text{ cm}^{-1}$  above this origin, whereas for  $^{18}\text{O}_2$  it will be  $0.07516\text{ cm}^{-1}$  below.

**Table 3**

Comparison of the spectroscopic parameters of the  $\nu = 0$  and 1 levels of the  $a^1\Delta_g$  state of  $^{16}\text{O}_2$ .

Parameters	$a^1\Delta_g$ state of $^{16}\text{O}_2$					
	This work	Amiot and Vergès [30]	Rothman [31]	Cheah et al. [14] <sup>c</sup>	Drouin et al. [20] <sup>c</sup>	HITRAN <sup>d</sup>
$T_0$	7883.756645(113) <sup>a</sup>	7883.76179(28) <sup>a</sup>	7882.4288(3) <sup>b</sup>	7888.107842(86) <sup>b</sup>		7883.75639 <sup>a</sup>
$B_0$	1.417839039(38)	1.41784020(82)	1.4178442(19)	1.41780381(90)	1.417798185(45)	1.41779818 <sup>c</sup>
$D_0$	$5.102256(243)\times 10^{-6}$	$5.1769(56)\times 10^{-6}$	$5.1074(24)\times 10^{-6}$	$5.11144(139)\times 10^{-6}$	$5.10196(34)\times 10^{-6}$	$5.10210^c$
$H_0$	$-2.395(283)\times 10^{-12}$	$1.589(89)\times 10^{-10}$			$-2.79(41)\times 10^{-12}$	
$T_1$	9367.208821(267) <sup>a</sup>		9365.881(28) <sup>b</sup>			9367.20879 <sup>a</sup>
$B_1$	1.40072433(17)		1.40051(42)			1.4007253
$D_1$	$5.1211(41)\times 10^{-6}$		$4.35(1.22)\times 10^{-6}$			$5.1263\times 10^{-6}$
$H_1$	$-4.97(313)\times 10^{-12}$					

### Notes

<sup>a</sup>)The energy origin is taken for the hypothetical  $N = 0, J = 1$  level of the ground  $X^3\Sigma_g^-$  state (see text for details).

<sup>b</sup>) The energy origin is taken for the level  $N = 1, J = 0$  of the ground  $X^3\Sigma_g^-$  state. The difference between the  $N = 1, J = 0$  and hypothetical  $N = 0, J = 1$  levels is  $0.24584\text{ cm}^{-1}$ .

<sup>c</sup>)The used Hamiltonian contains  $[J(J+1) - \mathcal{Q}^2]$  rather than just  $J(J+1)$  used in this work (Eq.2).

<sup>d</sup>)Constants taken from the program that was used to generate the most recent HITRAN line list. The rotational constants in the  $\nu=0$  state are those from Hillig et al [9], rotational constants in the  $\nu=1$  state and all term values are based on the unpublished FTS data of Brault [11].

**Table 4**

Spectroscopic parameters of the  $\nu = 0$  level of the  $X^3\Sigma_g^-$  and  $a^1\Delta_g$  states of  $^{16}\text{O}^{18}\text{O}$ ,  $^{16}\text{O}^{17}\text{O}$  and  $^{17}\text{O}^{18}\text{O}$ .

	$^{16}\text{O}^{18}\text{O}$		$^{16}\text{O}^{17}\text{O}$	$^{17}\text{O}^{18}\text{O}$
	$X^3\Sigma_g^-$			
<b><i>B</i></b>	1.3578522686(414)		1.39533197	1.31549483
<b><i>D</i></b>	$4.31692(53)\times 10^{-6}$		$4.5071\times 10^{-6}$	$4.023\times 10^{-6}$
<b><math>\lambda</math></b>	1.984674291(162)		1.98471102	1.98463280
<b><math>\lambda_D</math></b>	$1.833535(842)\times 10^{-6}$		$1.88847\times 10^{-6}$	$1.7827\times 10^{-6}$
<b><math>\lambda_H</math></b>	$9.50(81)\times 10^{-12}$			
<b><math>\gamma</math></b>	$-7.956001(11)\times 10^{-3}$		$-8.176597\times 10^{-3}$	$-7.70715\times 10^{-3}$
<b><math>\gamma_D</math></b>	$-7.318(15)\times 10^{-9}$		$-7.005\times 10^{-9}$	$-7.44\times 10^{-9}$
	$a^1\Delta_g$			
<b><i>T<sup>a)</sup></i></b>	7885.06789(13) <sup>b)</sup>		7884.4476(11)	7885.77532(63)
<b><i>B</i></b>	1.33913493(10)		1.3761054(91)	1.2973728(86)
<b><i>D</i></b>	$4.552623(674)\times 10^{-6}$		$4.795(16)\times 10^{-6}$	$4.2413(43)\times 10^{-6}$
<b><i>Number of lines</i></b>	MW: 85	This work: 208	This work: 51	This work: 140
<b><i>rms</i></b>	$6.73\times 10^{-2}$ MHz	$0.69\times 10^{-3}$ cm <sup>-1</sup>	$2.35\times 10^{-3}$ cm <sup>-1</sup>	$2.57\times 10^{-3}$ cm <sup>-1</sup>

**Notes**

Due to the hyperfine splitting affecting the transitions of the  $^{16}\text{O}^{17}\text{O}$  and  $^{17}\text{O}^{18}\text{O}$  species, the ground state rotational constants of these two species were fixed to the values obtained in the separate fit of the microwave data of Ref. [19] (see Text and Table 5).

<sup>a)</sup>The energy origin is taken for the level  $N = 0$ ,  $J = 1$  of the  $X^3\Sigma_g^-$  ground state (see text for details). The lowest energy level will be below this origin by a value of  $0.47795$  cm<sup>-1</sup> for  $^{16}\text{O}^{18}\text{O}$ ,  $0.46452$  cm<sup>-1</sup> for  $^{16}\text{O}^{17}\text{O}$  (if ignoring the hyperfine structure), and  $0.49403$  cm<sup>-1</sup> for  $^{17}\text{O}^{18}\text{O}$  (if also ignoring the hyperfine structure).

<sup>b)</sup> The term value used in HITRAN was  $7885.06858$  cm<sup>-1</sup> based on the unpublished FTS data of Brault [11].

**Table 5**

Spectroscopic parameters of the  $\nu = 0$  level of the  $X^3\Sigma_g^-$  state of  $^{16}\text{O}^{17}\text{O}$  and  $^{17}\text{O}^{18}\text{O}$  from a new fit of the data from Ref. [19].

Parameters	$^{16}\text{O}^{17}\text{O}$ (This work)	$^{16}\text{O}^{17}\text{O}$ [19]	$^{17}\text{O}^{18}\text{O}$ (This work)	$^{17}\text{O}^{18}\text{O}$ [19]
	$X^3\Sigma_g^-$			
$B$	1.39533197(324)	1.39531862(333)	1.31549483(247)	1.31549006(333)
$D^a$	$4.5071 \times 10^{-6}$	$4.623 \times 10^{-6}$	$4.023 \times 10^{-6}$	$4.102 \times 10^{-6}$
$\lambda$	1.98471102(30)	1.984709368(333)	1.98463280(148)	1.98463298(133)
$\lambda_D$	$1.88847(375) \times 10^{-6}$	$1.91799(667) \times 10^{-6}$	$1.7827(96) \times 10^{-6}$	$1.8012(167) \times 10^{-6}$
$\gamma$	$-8.176597(86) \times 10^{-3}$	$-8.176123(133) \times 10^{-3}$	$-7.70715(13) \times 10^{-3}$	$-7.706965(233) \times 10^{-3}$
$\gamma_D$	$-7.005(614) \times 10^{-9}$	$-8.0(10) \times 10^{-9}$	$-7.44(123) \times 10^{-9}$	$-9.01(200) \times 10^{-9}$
$b_F$ or $b^b$	$-1.826076(307) \times 10^{-3}$	$-3.383707(166) \times 10^{-3}$	$-1.82614(70) \times 10^{-3}$	$-3.384341(333) \times 10^{-3}$
$c$	$4.67255(79) \times 10^{-3}$	$4.66089(100) \times 10^{-3}$	$4.67277(287) \times 10^{-3}$	$4.6592(20) \times 10^{-3}$
$eQq$	$-2.713(80) \times 10^{-4}$	$-2.769(100)$	$-2.733(158) \times 10^{-4}$	$-2.602(167)$
Number of lines	59		30	
rms	0.039 MHz	0.06 MHz	0.042 MHz	0.07 MHz

**Notes**

<sup>a)</sup> In our fit the  $D$  constant was fixed to the one obtained in the preliminary fit of electronic data. In Ref [19] it was fixed to the value scaled from the principal isotopologue. See text for details.

<sup>b)</sup> In Ref. [19], hyperfine constants were fit to  $H_{hfs} = bI \cdot S + cI_z S_z + \frac{e^2 Qq(3I_z^2 - I(I+1))}{4I(2I-1)}$

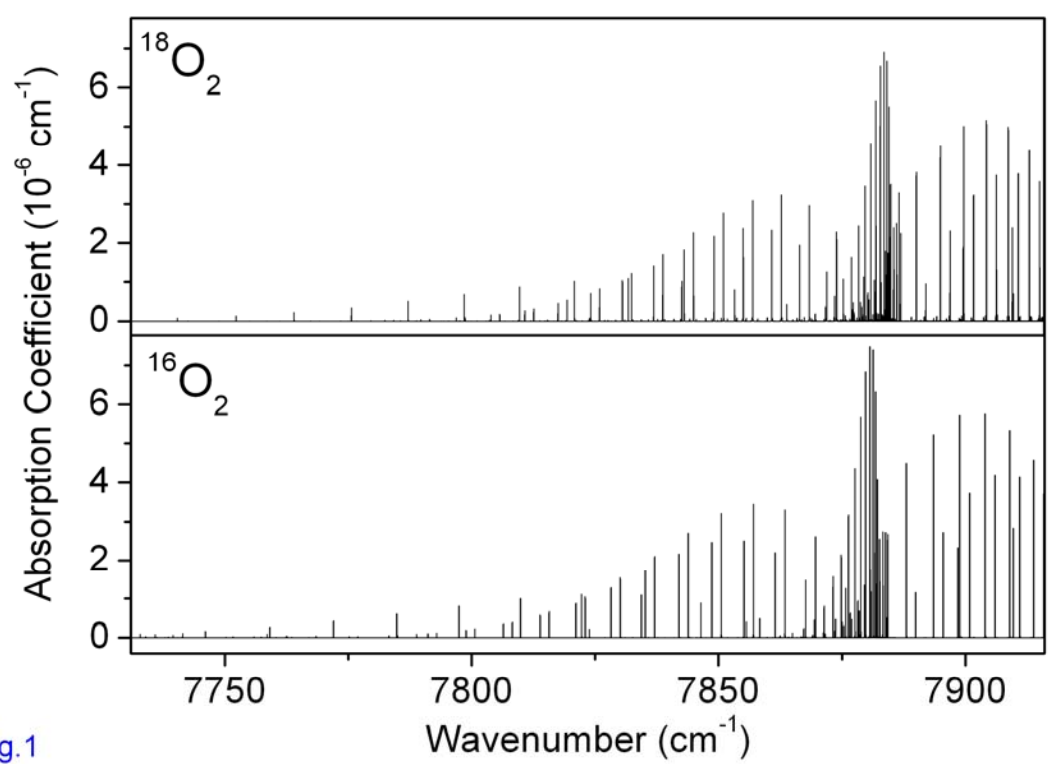


Fig.1

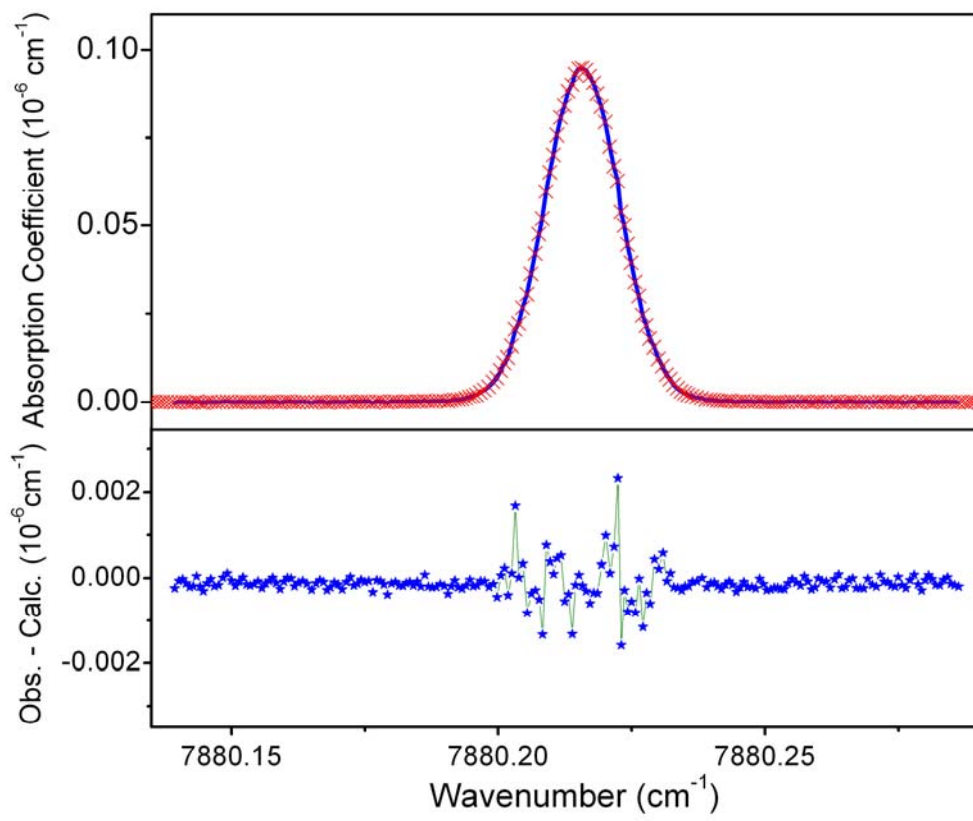


Fig.2

Fig.3

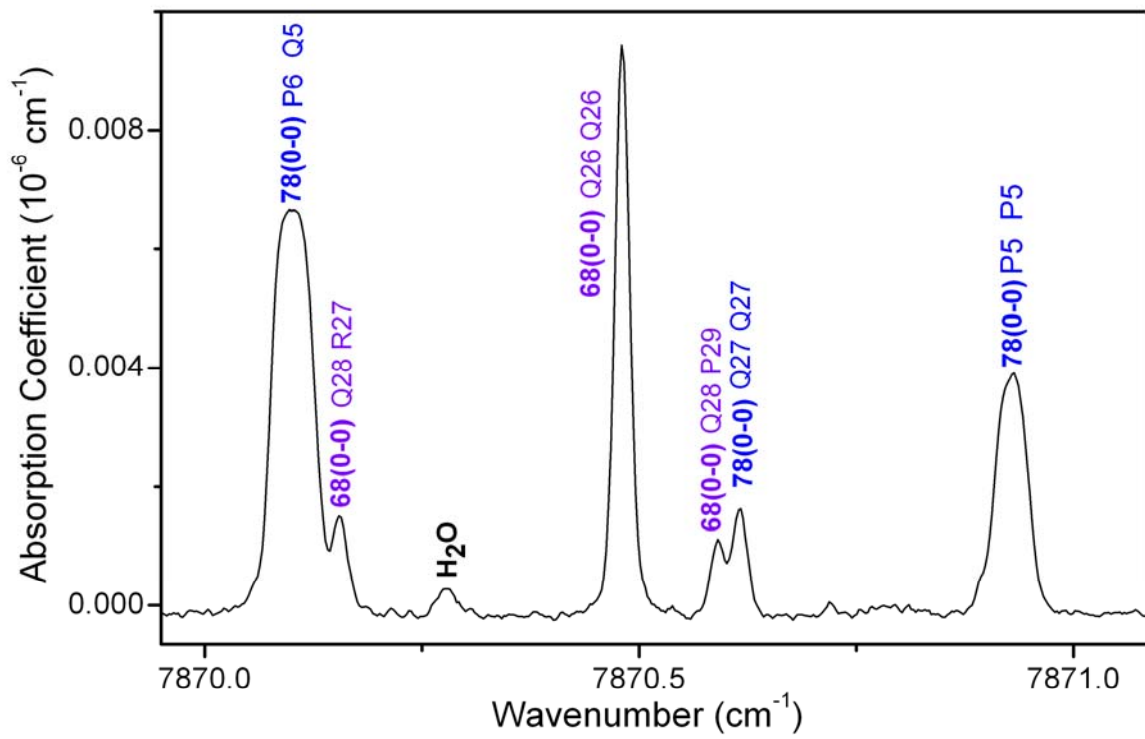


Fig.4

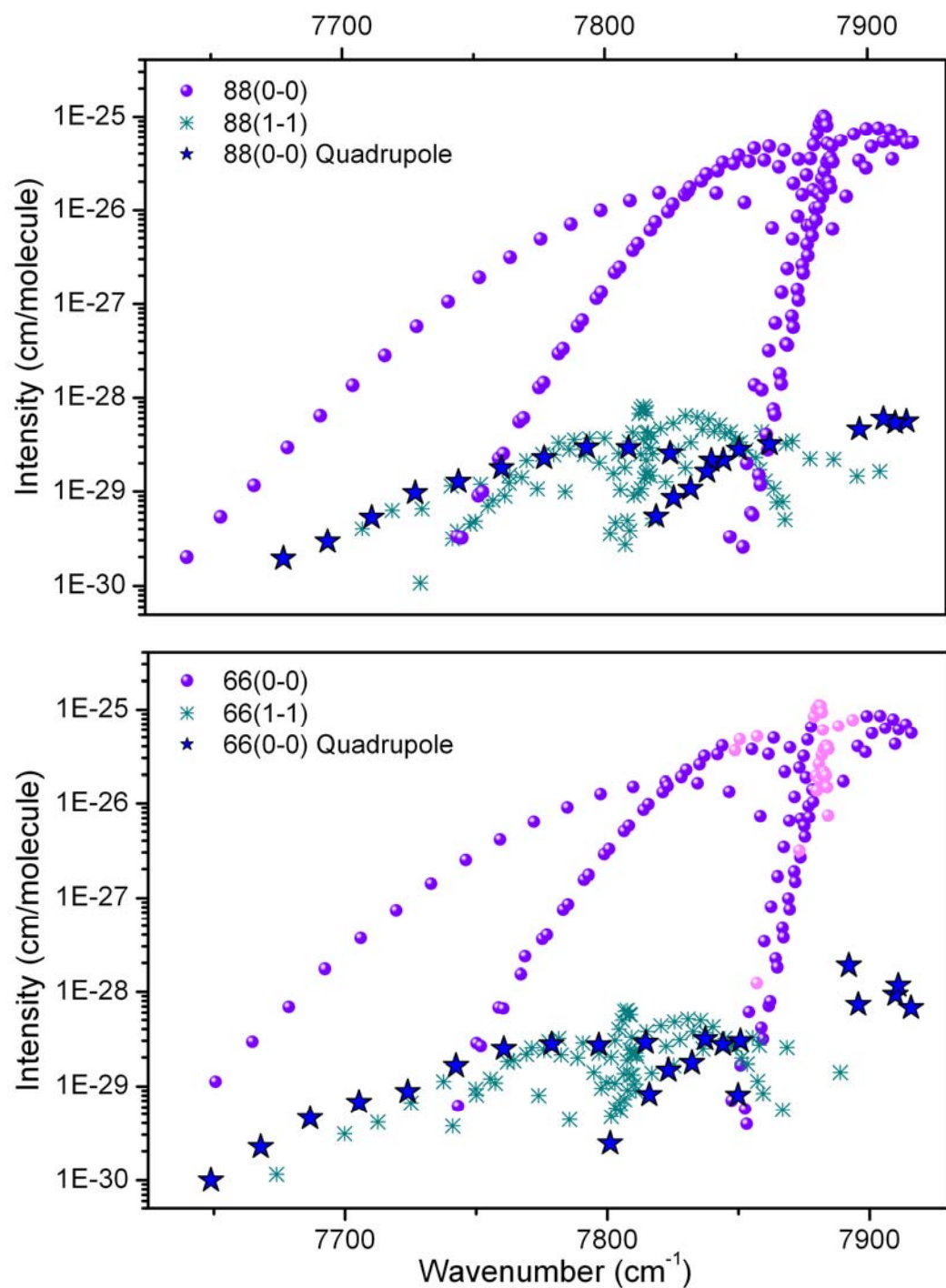


Fig.4

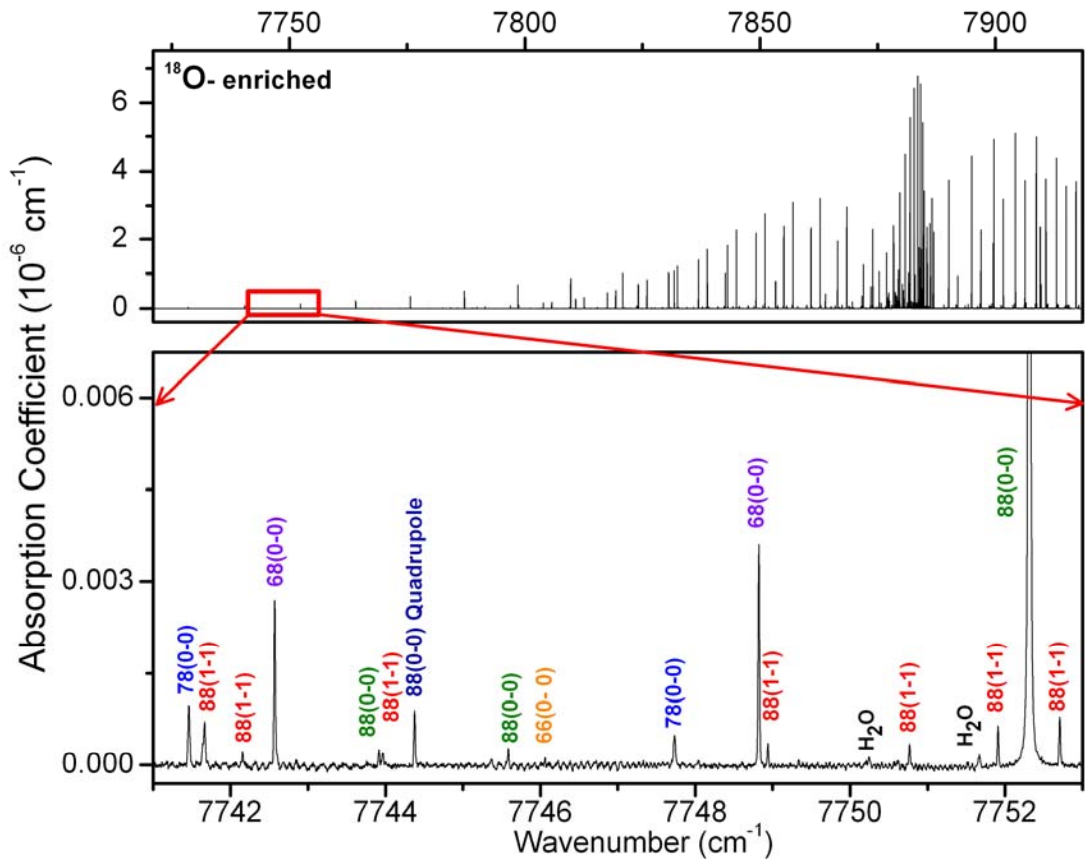


Fig.5

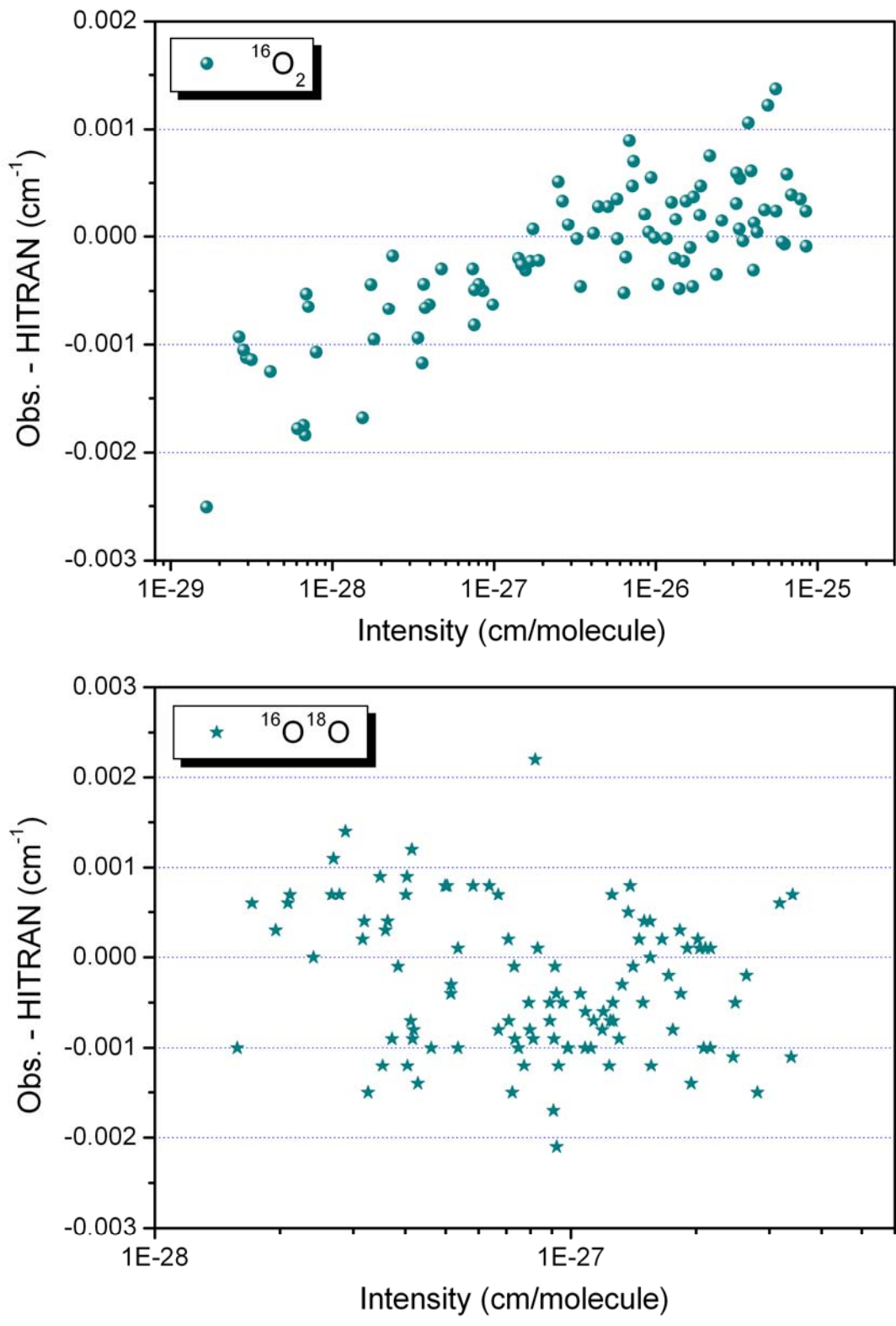


Fig. 6

e-component, for online publication only

[Click here to download e-component, for online publication only: 16O spectra\\_Global\\_linelist.txt](#)

e-component, for online publication only

[Click here to download e-component, for online publication only: 18O spectral\\_Global\\_linelist.txt](#)

e-component, for online publication only

[Click here to download e-component, for online publication only: 66\\_fit.txt](#)

e-component, for online publication only

[Click here to download e-component, for online publication only: 67\\_fit.txt](#)

e-component, for online publication only

[Click here to download e-component, for online publication only: 68\\_fit.txt](#)

e-component, for online publication only

[Click here to download e-component, for online publication only: 78\\_fit.txt](#)

e-component, for online publication only

[Click here to download e-component, for online publication only: 88\\_fit.txt](#)